Composites Part B 83 (2015) 7–13

Contents lists available at ScienceDirect

Composites Part B

journal homepage: www.elsevier.com/locate/compositesb

A dual-functional polymeric system combining shape memory with self-healing properties

Hongqiu Wei [a], Yongtao Yao [a], Yanju Liu [b], Jinsong Leng [a, *]

[a] Center for Composite Materials and Structures, Harbin Institute of Technology (HIT), Harbin 150080, People's Republic of China
[b] Department of Astronautical Science and Mechanics, Harbin Institute of Technology (HIT), Harbin 150080, People's Republic of China

ARTICLE INFO

Article history:
Received 6 December 2014
Received in revised form
15 April 2015
Accepted 6 August 2015
Available online 20 August 2015

Keywords:
A. Smart materials
A. Resins

ABSTRACT

With the aim of seeking a convenient way for integrating functional materials, a polymeric system, presenting both self-healing property and shape memory behavior, was proposed and constructed based on epoxy based shape memory polymer (ESMP) and poly (ε-caprolactone) (PCL). The synthesis principle of PCL–ESMP composite was based on phase separation phenomenon between the two ingredients. Such phase separated PCL–ESMP composite reserved melting transition of PCL and glassy transition of ESMP, respectively, which was the crucial mechanism for achieving self-healing performance and shape memory behavior. A bending-recovery experiment demonstrated that PCL–ESMP composite possessed excellent thermal-induced dual-shape memory effect. Meanwhile, single edge notched bend testing revealed that such composite exhibited desirable self-healing performance as well. This article introduced a simple contrivable concept and exhibited some experimental results of the PCL–ESMP dual-functional composite system. The promising applications are expected to more widely, such as functional composite matrix and intelligent structures.

1. Introduction

Stimulus-responsive materials based on polymer networks have been witnessed significant growth in the past decades, especially for the two branches, shape memory polymers (SMPs) and self-healing polymers (SHPs) [1]. SMPs are characterized for the shape memory effect (SME), which present the performance to revert the original shape from the provisional shape when they are triggered by external stimulus, such as heat [2–4], ultraviolet irradiation [5], electricity [6–8], water or moisture [9], and magnetic field [10], appropriately. Based on the unique capabilities, SMPs possess a broad applied range that changes from deployable structures and actuators to biomedical devices as well as sensors [11–15]. The other one, SHPs, inspired by the self-healing of organism, are known for the capability to self-repair from a physical crack or damage under certain external stimulus [16–18]. Self-healing performance not only reduces the cost of maintenance, but also endows high security and long service lifetime to the materials [19,20].

Both shape memory and self-healing are intelligent and promising characteristics. It has attracted increasingly interests of researchers to construct materials with both self-healing and shape memory properties [21–23]. Sodano presented polyurethanes based on Diels–Alder (DA) reaction exhibiting shape memory behavior and healed capabilities [21]. Wang also constructed a polymer network possessing both shape recovery and self-healing properties upon utilizing the cross-linking reaction between poly(vinyl butyral) (PVB) and hexamethylene diisocyanate (HDI) [22]. Both of them demonstrated that traditional materials exhibited smart behavior at the presence of SME. Moreover, self-healing performance could realize without the need of external forces. Such dual-functional polymeric systems present potential to broaden and enrich the developments of smart materials and structures.

Epoxy resin as a class of traditional engineering materials possesses a plenty of advantages, especially for the superior mechanical properties, chemical stabilities, excellent thermal and thermo-mechanical behaviors, etc. [24–26]. Recently, researches have concentrated on developing intelligent properties of epoxy resins to widen their applications as engineering smart materials and structures. Both epoxy based shape memory polymers (ESMP) [27–30] and self-healing epoxy systems [31–35] have been prepared successfully, however, it is more important to fabricate epoxy based polymer presenting both the two properties for smart systems. Mather et al. developed shape memory assisted self-healing

* Corresponding author. Tel./fax: +86 451 86402328.
E-mail address: lengjs@hit.edu.cn (J. Leng).

http://dx.doi.org/10.1016/j.compositesb.2015.08.019
1359-8368/

(SMASH) systems recently [36,37]. They reported a SMASH coating achieving via spin-coating ESMP on electrospinning poly(ε-caprolactone) (PCL) membrane [36]. In this composite, once cracks or damages generated, PCL fibers could melt and flow to heal the damages with the assistance of SME to close the cracks by heating. Even through the study only focused on a coating, the method they mentioned paved the way for the developments of smart epoxy-based materials.

Inspired by the researches above, a thermoset–thermoplastic polymeric system, consisting of ESMP and PCL, was utilized to fabricate a kind of materials with thermally-induced dual-shape memory and self-healing properties in this study. ESMP and PCL constructed a phase separated composite, so that the two ingredients could reserve their original performance, which guaranteed the achievement of shape memory and self-healing. The chemical and morphology structure were investigated with Fourier Transform Infrared Spectroscopy (FTIR) and Scanning Electron Microscopy (SEM). Thermo-mechanical performances of the materials were presented by Dynamic Mechanical Analysis (DMA). In what follows, the smart capabilities, self-healing capacity and shape memory behavior, were evaluated by Single Edge Notched Bend (SENB) and Bending-recovery test in detail.

2. Experimental details

2.1. Materials

The polymer matrix was ESMP, which was fabricated as presented in our previous report [28]. The thermoplastic poly (ε-caprolactone) (PCL) pellets purchased from Perstorp Chemical Trading Co., Ltd. (CaPa 6500, Mn = 40,000–50,000; density: 1.146 g/mL) were chosen as healing agent. All materials were used as received without further treatment.

2.2. Fabrication of PCL–ESMP composites

Different weight ratios of epoxy based resin and PCL pellets were added in a 500 mL flask and stirred constantly at 80 °C. Two hours later, curing agent was added and stirred continuously for another 30 min to obtain a homogeneous PCL–ESMP mixture. In order to remove bubbles, the above mixture was degassed at a vacuum oven for 15 min at 80 °C, then, inserted into the preheated glass molds. The curing condition was set as follows: 80 °C for 3 h, 100 °C for 3 h and 150 °C for 5 h. The fully cured materials were cooled down to room temperature at a rate of 20 °C/min. Finally, the PCL–ESMP composites were obtained. The nomenclature and content of each component were shown in Table 1. The fabricated PCL–ESMP composite was defined as Px, which meant the mass ratio of PCL/ESMP was x/100, and the PCL content was treated as x *wt%*.

2.3. Characterizations

A Fourier Transform Infrared Spectroscopy (FTIR) (Spectrum One, Perkin Elmer) was employed to analysis the reaction between PCL and ESMP during the curing process. The sample was powder and prepared by KBr pellets. The test condition was used a spectral range of 4000–370 $cm^{-1}$and a resolution of 4 cm^{-1}.

Scanning Electron Microscopy (SEM) (Quanta 200FEG) was used to discuss the morphologies of (I) the cracks of the samples before after healing (II) the fractured surfaces of the samples. In order to investigate morphology of phase separation, completely cured specimens were quickly fractured in liquid nitrogen and then immersed in chloroform for 30 min to eliminate PCL ingredient. All the SEM samples were sputter-coated with gold before testing.

Dynamic Thermo-mechanical Analyzer (DMA/SDTA861e, Mettler–Toledo) was conducted by tension mode at a frequency of 1 Hz and 0.05% strain. The test temperature ranged from 25 °C to 250 °C with a heating rate of 5 °C/min.

Single Edge Notched Bend (SENB) testing was conducted by ASTM D5045 to evaluate self-healing ability. The test was under a three-point mode with a span of 40 mm and a cross-head speed of 1 mm/min (Zwick/Roell instrument). The specimen ($50 \times 10 \times 5$ mm^3) with a 3 mm notch in center was obtained by laser cutting machine, after that razor blade was used to generate a 2 mm deep pre-crack. Such pre-crack sample was loaded until the point which was 90% loss of the peak load, then, it was healed for 30 min at a certain temperature, 84 °C, 104 °C, 124 °C, or 144 °C, respectively, in an oven. Such healed sample was cooled to room temperature at a rate of 20 °C/min. In order to characterize the healing efficiency of PCL–ESMP, the sample was re-loaded to failure according to the procedure described above. The original and post healing maximum loads were required to calculate the healing efficiency. The equation was as follows [18,31]:

$$\text{Healing efficiency}(\%) = \frac{\text{Max. Load}_{\text{healed}}}{\text{Max. Load}_{\text{original}}} \times 100\% \quad (1)$$

Shape memory behavior of PCL–ESMP was investigated by a bending-recovery test. A strip with dimension of $50 \times 5 \times 1$ mm^3 was performed as original shape. It was bended into a "U" shape as its temporary shape at $T_g + 20$ °C. The "U" shape sample was fixed by cooling down the sample to room temperature at a rate of 20 °C/min. When deformed sample was re-heated above $T_g + 20$ °C, it could recovery to the original shape. Shape recovery ratio (Rr) and shape recover speed (Rs) were employed for characterizing the shape memory behavior of PCL–ESMP. Rr was defined as $Rr = \theta r/180°$, where θr was obtained by measuring the released angle after the recover process. Rs was determined by the recovery time.

3. Results and discussions

3.1. Structural characterization

FTIR spectrum ranging from 4000 to 370 cm^{-1} was employed to analyze the interaction between PCL and ESMP. From Fig. 1, it is clear that PCL–ESMP composites have same characteristic absorption peaks, indicating those materials have same functional groups. The absorption peaks at 2946 cm^{-1} and 2870 cm^{-1} are corresponding to $-CH_2-$. A sharp absorption peak appears at 1733 cm^{-1} belongs to –C=O– groups. The absorption peak at 1455 cm^{-1} is assigned to the stretch vibration of C–H bonds. The absorption peak at 1182 cm^{-1} is pertained to the C–O bonds, and the absorption peak at 1363 cm^{-1} demonstrates that the C–O bonds are attached to cyclic anhydride [28]. All these characteristic absorption peaks belong to either ESMP or PCL. It reveals that no new characteristic absorption peaks emerge between ESMP and PCL. So there is only physical reaction between them during the curing process. It is the basis for phase separation phenomenon.

To reveal the phase separated morphology of polymers, some microscopy techniques have already been presented [38]. In this

Table 1
Compositions of the PCL–ESMP composites.

Samples	Epoxy based resin (g)	Curing agent (g)	PCL (g)	PCL/ESMP (*wt%*)
ESMP	100	83.6	0	0
P6.1	90	75.24	10	6.1
P13.6	80	66.88	20	13.6
P23.3	70	58.52	30	23.3

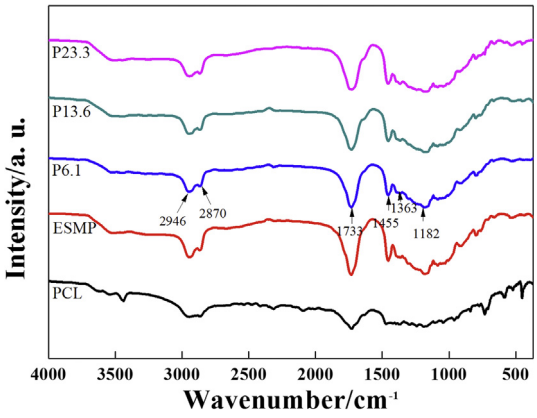

Fig. 1. FTIR spectra of ESMP, P6.1, P13.6, P23.3 and PCL.

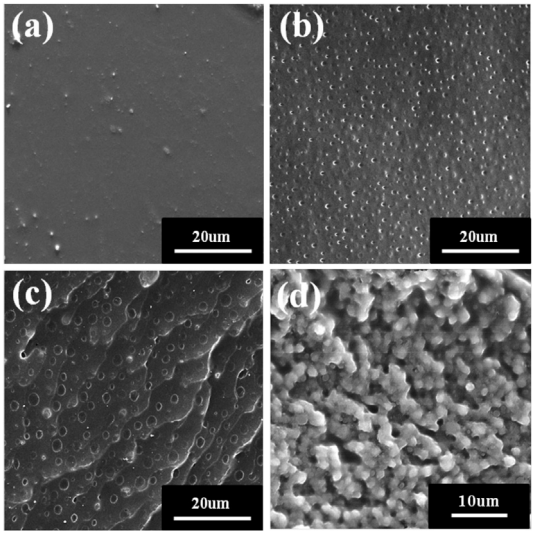

Fig. 2. SEM images of fractured surfaces of different composition PCL–ESMP composites: (a) ESMP (b) P6.1 (c) P13.6 (d) P23.3.

study, SEM was employed to investigate the morphology of the PCL–ESMP blend. SEM images of fractured surfaces of PCL–ESMP after treatment with chloroform are presented in Fig. 2. Because chloroform is an excellent solvent of PCL, only ESMP phase and residual PCL phase are visible in the surfaces. Fig. 2a shows a smooth and neat surface, because chloroform has no effect on pure ESMP. From Fig. 2b–d, the morphologies of PCL–ESMP become quite complex, "particle/matrix" phenomenon appearing on the treated surfaces. Further investigation reveals that when PCL content is less than 23.3 *wt%*, PCL phase presents spherical particles dispersing in ESMP matrix (Fig. 2b, c). As PCL content increasing to 23.3 *wt%*, the phase structure has a significant invert. ESMP phase changes into spheres, and the residual PCL with irregular shape starts to be the "matrix" to concatenate these ESMP "particles" (Fig. 2d). The results are similar with previous studies. It is the evidence for the occurrence of phase separation [39,40]. Although PCL phase and ESMP phase display different forms in PCL–ESMP composites, SEM results verify that PCL and ESMP formed a phase separated structure.

3.2. Thermal properties

To investigate the thermo-mechanical capability and viscoelastic behavior of the PCL–ESMP composites, dynamical mechanical analysis (DMA) experiment was performed. The curves of storage module and loss factor (tan δ) data as a function of temperature are presented in Fig. 3. It shows that pure ESMP mainly has two plateaus which are corresponding to the glassy state at low temperature and the rubbery state at high temperature, respectively. Between the two plateaus, sudden drop can be observed distinctly. For PCL–ESMP composites, glassy platforms also appear at the low temperature. However, with the temperature further elevating, intermediate plateaus around 60 °C gradually emerge instead of sharp decreasing to rubbery state, which is attributed to the melt of thermoplastic PCL (64 °C). Clearly, storage modulus of PCL–ESMP blends reduce as the increasing PCL content. It is attributed to that storage modulus of pure PCL is far lower than pure ESMP (Fig. 3a). Furthermore, the increasing PCL contents induce longer spaces between the cross-linking net points of ESMP leading to lower steric hindrance, which is also a crucial reason resulting in the declining storage modulus [41,42].

Peak value of the tan δ (Fig. 3b) is conducted as a reference for phase transition temperature [2,3]. It is easy to note that only one peak can be observed in the pure ESMP curve, representing for the T_g of ESMP. For PCL–ESMP blend, it is clear that all the tan δ curves show two separated thermal transitions, belonging to the melting transition of PCL and the glass transition of ESMP, respectively. The isolated T_m of PCL and T_g of ESMP demonstrate the PCL and ESMP are phase separated [39,43], which means PCL–ESMP composite can obtain both self-healing and shape memory properties. With increasing PCL content, T_m and T_g present downward trends, which are similar with previous study [3,22,41]. The declining T_m is mainly contributed by two aspects. One is that, as PCL content increasing, effect of PCL on the thermo-mechanical properties of the PCL–ESMP composites is more significant. The second, it should be

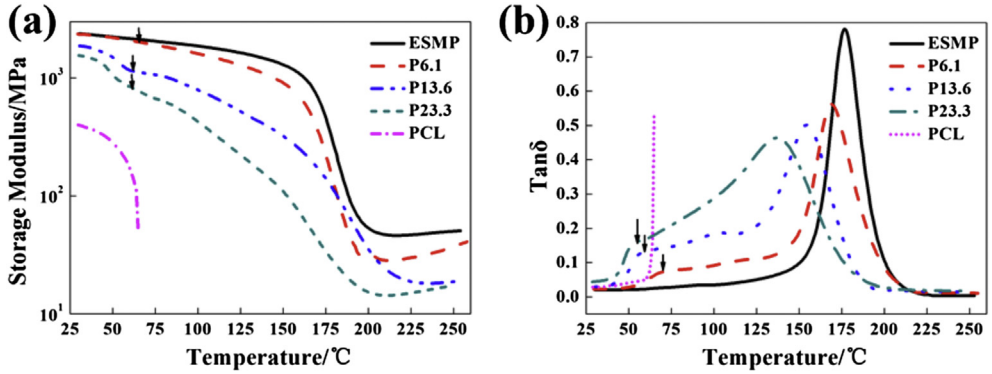

Fig. 3. DMA curves of ESMP, P6.1, P13.6, P23.3, PCL (a) storage modulus as a function of temperature and (b) tangent delta as a function of temperature.

Table 2
Summary of properties determined by DMA experiment.

Sample	[a]E_g/GPa	[b]E_i/GPa	[c]E_r/GPa	[d]T_m/°C	[e]T_g/°C
ESMP	2.38	–	0.048	–	176.1
P6.1	2.35	1.97	0.033	67.8	168.9
P13.6	1.87	1.13	0.018	59.0	154.7
P23.3	1.56	0.8	0.017	55.0	137.1
PCL	0.40	–	–	64.0	–

[a] E_g: storage modulus of glassy state (30 °C).
[b] E_i: storage modulus of intermediate state (64 °C).
[c] E_r: Storage modulus of rubbery state.
[d] T_m: melting transition temperature.
[e] T_g: glassy transition temperature.

contributed by the increasing PCL content induces decreasing T_g and wider tan δ peak of ESMP. For sample with more PCL content, the glass transition of ESMP phase occurs much earlier. Combining these two reasons, T_m increases as PCL content reducing. The decrease of T_g is attributed to the PCL phase disturbs the inter-chain interactions of ESMP in PCL–ESMP system, which increases spaces between the cross-linking net points of ESMP, finally, resulting in the decreasing density of cross-linking points [41,42].

As stated, DMA results indicate that the storage modulus decreases visibly, T_m and T_g turn into a relative low temperature, and two independent thermal transitions emerge gradually, as the PCL content increasing. Particular results of DMA are summarized in Table 2.

3.3. Effect of PCL component on composite mechanical properties

The original strategy of modifying materials should obey that incorporation of inclusion should not have negative effects on the material's intrinsic properties, including physical performances. SENB geometry according to ASTM D5045 is conducted to assess the effect of PCL on PCL–ESMP composite under three-point bending mode. Pure ESMP as a typical kind of thermosetting polymers presents highly brittle mechanical behavior. Thermoplastic PCL structurally consists of flexible linear aliphatic segments, which endows it excellent ductile performances. For the phase-separated PCL–ESMP blends, P6.1 and P13.3 directly break into two halves, which is the same with the fracture mode of pure ESMP. P23.3 just appears a large-scale crack indicating the ductile fracture mode that is similar to PCL. It can be summarized as the mechanical properties of PCL–ESMP blends change to toughness from brittleness gradually with PCL content increasing (Fig. 4a, b). Such variation is closely related to their different phase separated morphologies showing in Fig. 2. At lower PCL content (P6.1 and P13.3), ESMP phase is the "matrix", while PCL phase acts as "spherical fillers" (Fig. 2b, c). The morphology indicates mechanical properties of ESMP occupy the dominant role, resulting in the brittle properties. At higher PCL content (P23.3), ESMP phase inverts to "spherical fillers", while PCL phase becomes "matrix" (Fig. 2d). Thus, ductile mechanical properties appear, owing to the important effect of flexible PCL "matrix" on the mechanical properties.

Further analysis find that, the fracture strength of PCL–ESMP ascends at first, and then decreases (Fig. 4c). Nevertheless, fracture strength of the PCL–ESMP composites are higher than pure ESMP, demonstrating the toughening effect of phase separation on thermosetting resin [44]. Herein, P23.3 presents a ductile performance which is an excellent balance between mechanical capabilities and self-healing abilities. So it is chosen for the following study.

3.4. Shape memory behavior of PCL–ESMP composites

Thermally-actuated shape memory behavior of P23.3 was characterized under a bending-recovery experiment, and ESMP was employed as contract test. In order to make the molecule

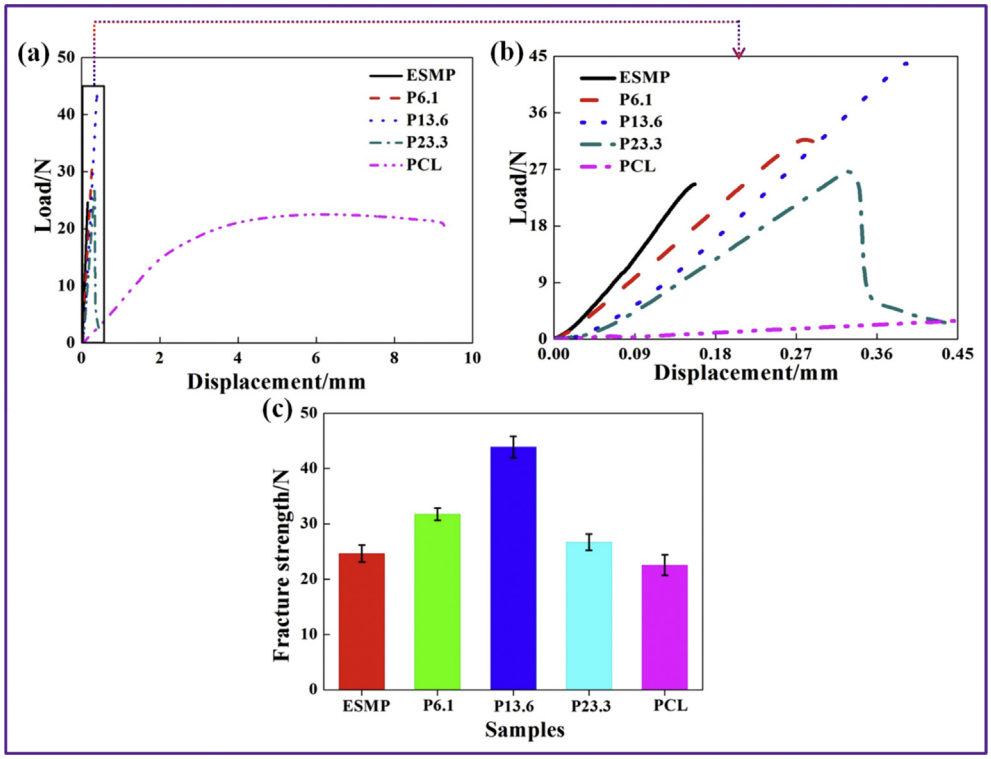

Fig. 4. Typical load–displacement curves (a), (b) (figure b is a magnification for the selected area in figure a) and fracture strength column diagram (c) of ESMP, P6.1, P13.6, P23.3. The results in (c) represent for average of three samples.

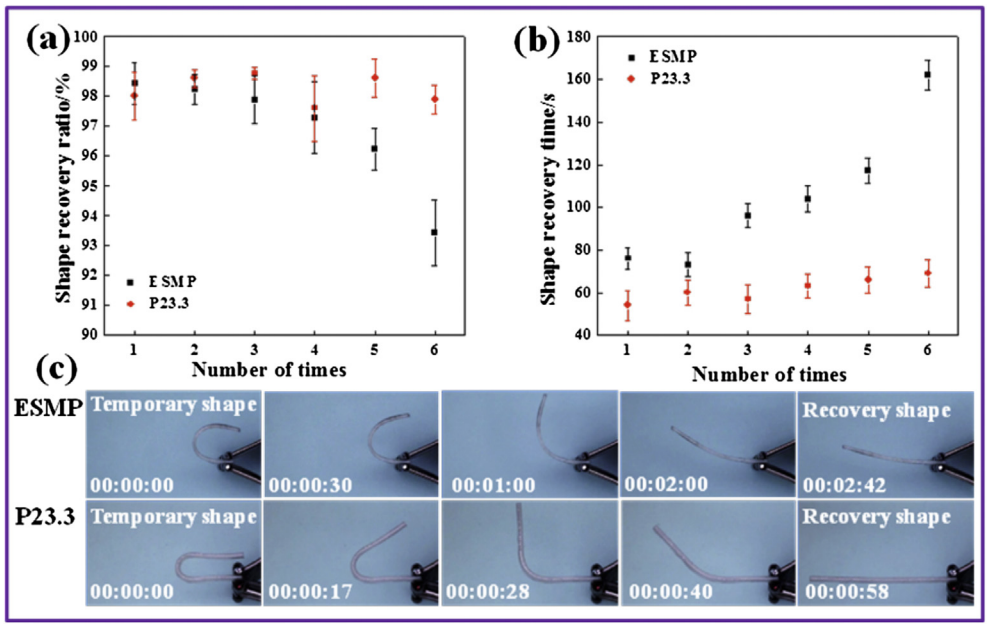

Fig. 5. Bending-recovery test results for samples ESMP and P23.3: (a) shape recover ratio (b) shape recover times (c) visual demonstration of ESMP's and P23.3's shape memory effect after six shape recovery cycles.

segments in a more activated status, the recovery temperatures of ESMP and P23.3 are set at their respective $T_g + 20$ °C. Fig. 5 presents shape recovery process of ESMP and P23.3, respectively. *Rr* of ESMP increases from 93.44% to 98.44% with increasing experimental times. P23.3 shows more stable and higher *Rr* than ESMP. It is still above 97% after six times of shape recovery, and mostly higher than 98% (Fig. 5a). In Fig. 5b, *Rs* of ESMP shows a markedly ascendant trend rising from 73 s to 162 s, while P23.3 completes the shape recovery cycles less than 80 s after six times of trials. The visual demonstration of the sixth shape recovery cycle of ESMP and P23.3 is exhibited in Fig. 5c. It offers a directly proof that both the flexibility and shape recovery cycle of P23.3 are superior to ESMP. The experimental results prove the introduction of PCL into ESMP can optimize shape memory properties of ESMP. As reported, molecule segments and crosslinking points play the roles of reversible phase and fixed phase, respectively, which are attributed to the SME in

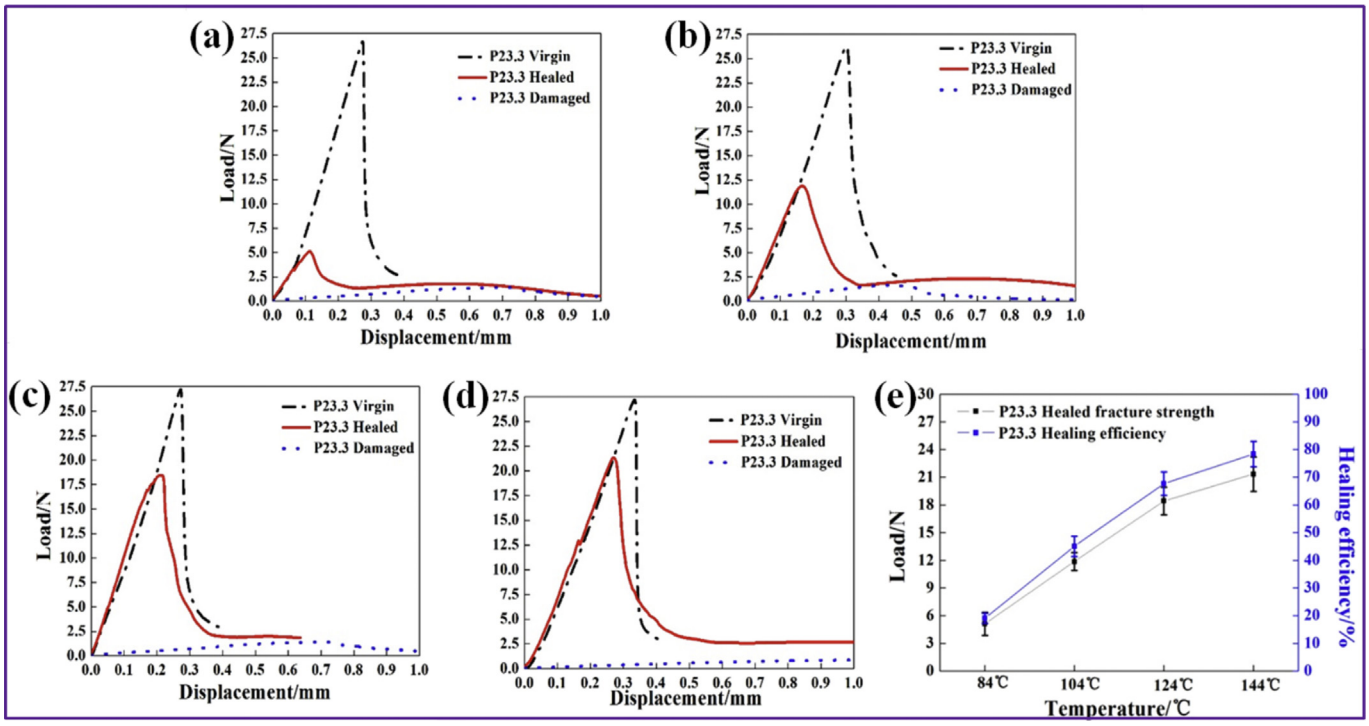

Fig. 6. Typical load–displacement curves for virgin, damaged and healed SENB specimens. Load SENBs to failure and then heal for 30 min under various temperature of (a) 84 °C, (b) 104 °C, (c) 124 °C, and (d) 144 °C. After cooling down, the samples were loaded again. The fracture strength of healed SENBs and healing efficiency are displayed in (e) as a function of temperature. Every spot in (e) stands for average result of three samples.

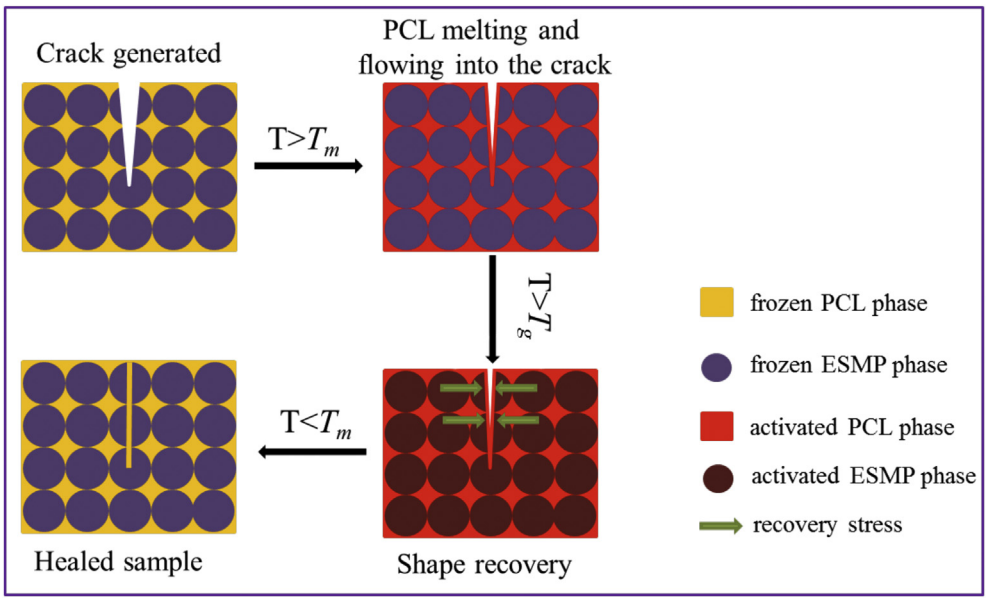

Fig. 7. Schematic description of a self-healing process combing shape memory.

thermosetting SMPs. Deformations of thermosetting SMPs mainly rely on reversible phase [12,13]. The appearance of PCL increases the quantity of movable molecule segments in the polymeric system, leading to the easy distortion and fast recovery of the P23.3. Higher *Rr*, faster *Rs* and better shape fixing make the samples P23.3 more suitable for practical applications.

3.5. Self-healing capacities of PCL–ESMP composites

As demonstrated in Fig. 4, P23.3 presents a relative slow and controlled crack based on the ductile behavior. Instead of breaking into two parts, just a large scale damage generates after test, which indicates P23.3 having the feasibility to be healed in the future. Therefore, P23.3 is used to analyze the self-healing performance quantitatively according to the process which has been mentioned in Experimental Section. Needing to emphasize here is that healing temperature (T_h) should higher than T_m (64 °C) of PCL to achieve liquidity of PCL. Four temperatures, 84 °C (T_m + 20 °C), 104 °C (T_m + 40 °C), 124 °C (T_m + 60 °C) and 144 °C (T_m + 80 °C) are chosen as T_h. A group of exemplary load–displacement curves of virgin (specimens contained a pre-crack), damaged (virgin specimens which have been load to generate a structure-scale crack), and healed (damaged specimens which have been healed for 30 min at T_h) SENBs are shown in Fig. 6a–d. The effect of T_h on healing capabilities is investigated.

As in Fig. 6e, the maximum load of healed samples at different T_h are 5.12 N, 11.87 N, 18.43 N and 21.34 N, respectively. According to equation (1), healing efficiencies are 19.07%, 45.07%, 67.68%, and

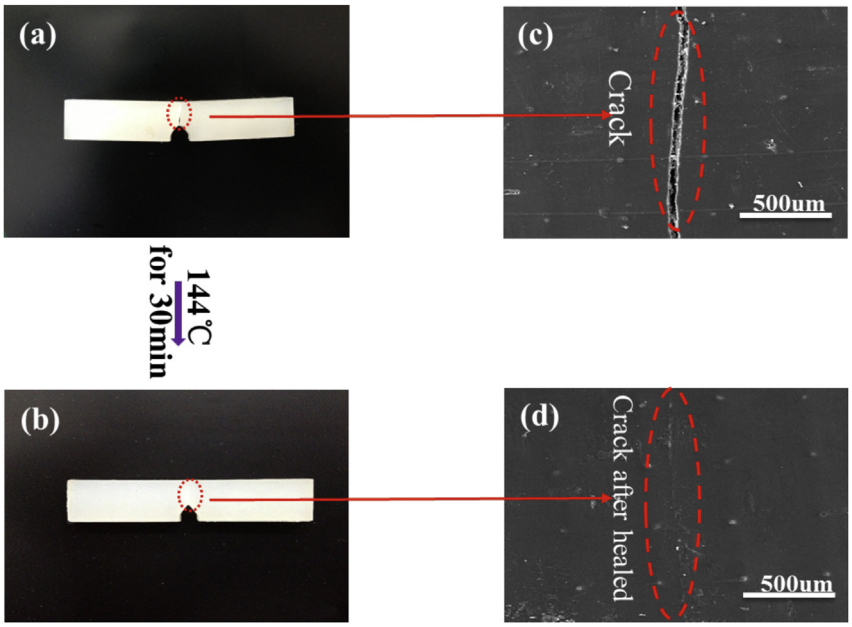

Fig. 8. Macroscopic pictures and SEM top views of a SENB specimen's surface after three point bending test (a, c) and after the thermal mending process without external pressure (b, d).

78.40%, respectively, which rise with increased T_h. The highest healing efficiency 78.40% is obtained at 144 °C. There are two mainly reasons contributed to the result. The first one is considered that higher T_h leads to lower viscosity and better liquidity of PCL, which is more important for the realization of self-healing [45]. Meanwhile, SME also plays a crucial role as previous researches presenting [21–23]. When T_h (84 °C and 104 °C) below T_g of P23.3, although the melting transition of PCL takes place, the ESMP phase is still in glassy state, indicating chain segments of ESMP are frozen. Due to the physical interactions between these two ingredients, frozen ESMP phase constrains the movements of PCL chains to some extent, resulting in the low healing efficiencies. Once T_h is set at 124 °C or 144 °C, suggesting T_h quite approaches or is higher than T_g of P23.3, ESMP phase is activated. On the one hand, the movements of ESMP chain segments are beneficial to the flowing action of PCL. On the other hand, the activated ESMP chain segments release the internal stresses that generate from three-bending test. These recovery forces bring the surfaces of crack together, which is necessary for the occurrence of self-healing. Therefore, high healing efficiencies can be obtained at high T_h without any external forces, especially for T_h higher than T_g. The schematic description of the healing process at T_h higher than T_g are displayed in Fig. 7.

In order to identify the healing process, the sample with the highest healing efficiency is employed to observe the status of crack before and after healing (Fig. 8). The macroscopic pictures (Fig. 8a, b) expressly present that the structure-scale crack disappears after healing for 30 min at 144 °C. Such results is consistent with SEM top surface images of the crack before (Fig. 8c) and after heating to repair (Fig. 8d). The visualization of crack repairing process demonstrates the realization of self-healing. The results illustrate that heating alone without any pressure or manual intervention can recovery major of load in the dual-functional system. For damage in structure-scale damage, it is a desirable performance.

4. Conclusions

A smart material, a shape memory composite with self-healing capability, was been proposed and fabricated successfully based on ESMP and PCL. ESMP and PCL constructed a phase separated polymeric system, benefiting the melting transition of PCL and the glassy transition of ESMP, which was the crucial factor for self-healing property and shape memory behavior. Results revealed that when the PCL content was 23.3 *wt%*, the PCL–ESMP composite presented superior overall properties. The bending-recovery experiment demonstrated that the shape recovery time was less than 80 s, and the recovery ratio was nearly 98% even after six times of shape recovery test. SENB test confirmed that healing efficiency was elevated with increasing healing temperature, and a desirable healing behavior obtained at the temperature higher than T_g without external forces. Such dual-function makes PCL–ESMP composite good candidates for functional composite matrix or intelligent structures, which can attract more interests of researchers.

Acknowledgments

This work is supported by the National Natural Science Foundation of China (Grant Nos 11225211, 11272106), for which we are very grateful.

References

[1] Seiffert S, Sprakel J. Chem Soc Rev 2012;41:909–30.
[2] Lee BS, Chun BC, Chung YC, Sul KI, Cho JW. Macromolecules 2001;34:6431–7.
[3] Shumaker JA, McClung AJW, Baur JW. Polymer 2012;53:4637–42.
[4] Jing X, Mi HY, Peng XF, Turng LS. Polym Eng Sci 2015;55:70–80.
[5] Lee KM, Koerner H, Vaia R, Bunning T, White T. Soft Matter 2011;7:4318–24.
[6] Liu YJ, Lv HB, Lan X, Leng JS, Du SY. Compos Sci Technol 2009;69:2064–8.
[7] Du FP, Ye EZ, Yang W, Shen TH, Tang CY, Xie XL, et al. Compos Part B Eng 2015;68:170–5.
[8] Lv HB, Huang WM, Leng JS. Compos Part B Eng 2014;62:1–4.
[9] Wang L, Yang XF, Chen HM, Yang G, Gong T, Li WB, et al. Polym Chem UK 2013;4:4461–8.
[10] Zhang SD, Li YF, Peng LQ, Li QF, Chen SL, Hou K. Compos Part A Appl Sci 2013;55:94–101.
[11] Lendlein A, Langer R. Science 2002;96:1673–6.
[12] Leng JS, LanX Liu YJ, Du SY. Prog Mater Sci 2011;56:1077–135.
[13] Meng QH, Hu JL. Compos Part A Appl Sci 2009;40:1661–72.
[14] Ratna D, Karger-Kocsis J. J Mater Sci 2008;1:254–69.
[15] Zhang L, Du HY, Liu LW, Liu YJ, Leng JS. Compos Part B Eng 2013;59:230–7.
[16] White SR, Sottos NR, Geubelle PH. Nature 2001;409:794–7.
[17] Hager M, Greil P, Leyens C, Zwaag S, Schubert U. Adv Mater 2010;22:5424–30.
[18] Yang Y, Urban MW. Chem Soc Rev 2013;42:7446–67.
[19] Zhang MQ, Rong MZ. Sci China Chem 2012;55:648–76.
[20] Mauldin TC, Kessler MR. Int Mater Rev 2010;6:317–46.
[21] Heo Y, Sodano H. Adv Funct Mater 2014;24:5261–8.
[22] Bai YK, Chen Y, Wang QH, Wang TM. J Mater Chem A 2014;6:9169–77.
[23] Nji J, Li GQ. Polymer 2010;51:6021–9.
[24] Paluvai NR, Mohanty S, Nayak SK. Polym Plast Technol 2014;53:1723–58.
[25] Dong CS, Davis IJ. Compos Part B Eng 2015;72:65–71.
[26] Withers GJ, Yu Y, Khabashesku VN, Cercone L, Hadjiev VG, Souza JM, et al. Compos Part B Eng 2015;75:175–82.
[27] Rousseau IA, Xie T. J Mater Chem A 2010;20:3431–41.
[28] Leng JS, Wu XL, Liu YJ. Smart Mater Struct 2009;18. 095031.
[29] Leonardi AB, Fasce LA, Zucchi IA, Hoppe CE, Soule ER, Perez CJ, et al. Eur Polym J 2011;47:362–9.
[30] Ahn D, Ding YF, Qi HJ. J Eng Mater Trans ASME 2011;133:021–5.
[31] Hamilton AR, Sottos NR, White SR. Adv Mater 2010;45:5159–63.
[32] Meure S, Wu DY, Furman S. Acta Mater 2009;57:4312–20.
[33] Blaiszika BJ, Sottos NR, White SR. Compos Sci Technol 2008;3:978–86.
[34] Pang JWC, Bond IP. Compos Sci Technol 2002;65:1797–9.
[35] Li Q, Siddaramaiah Kim NH, Hui D, Lee JH. Compos Part B Eng 2013;55:79–85.
[36] Rodriguez ED, Luo XF, Mather PT. ACS Appl Mater Inter 2011;3:152–61.
[37] Luo XF, Mather PT. ACS Macro Lett 2013;2:152–6.
[38] Guise O, Strom C, Preschilla N. Polymer 2011;52:1278–85.
[39] Chen JL, Chang FC. Macromolecules 1999;32:5348–56.
[40] Vanden PG, Goossens S, Goderis B, Groeninckx G. Polymer 2005;46:10758–71.
[41] Wang WX, Lv HB, Liu YJ, Leng JS. J Mater Chem A 2014;15:5441–9.
[42] Kazakeviciute-Makovska R, Mogharebi S, Steeb H, Eggeler G, Neuking K. Adv Eng Mater 2013;15:732–9.
[43] Torbati AH, Nejad HB, Ponce M, Sutton JP, Mater PT. Soft Matter 2014;10:3112–21.
[44] Luo XF, Ou RQ, Eberly DE, Singhal A, Viratyaporn W, Mather PT. ACS Appl Mater Interface 2010;1:612–20.
[45] Burattini S, Greenland BW, Chappell D, Colquhoun HM, Hayes W. Chem Soc Rev 2010;39:1973–85.